Towards a Machine-Learning-Assisted Dielectric Sensing Platform for Point-of-Care Wound Monitoring

Article *in* IEEE Sensors Letters · June 2020

DOI: 10.1109/LSENS.2020.2999031

10 authors, including:

Hamed Rahmani
Qualcomm
9 PUBLICATIONS **35** CITATIONS
SEE PROFILE

Maani Archang
University of California, Los Angeles
15 PUBLICATIONS **162** CITATIONS
SEE PROFILE

Babak Jamali
University of California, Los Angeles
17 PUBLICATIONS **54** CITATIONS
SEE PROFILE

Mahdi Forghani
University of California, Los Angeles
3 PUBLICATIONS **1** CITATION
SEE PROFILE

Sensor systems

Towards a Machine-Learning-Assisted Dielectric Sensing Platform for Point-of-Care Wound Monitoring

Hamed Rahmani[*,**], Maani M. Archang[*,†], Babak Jamali[*,***], Mahdi Forghani[*,**], Aaron M. Ambrus[†], Deeban Ramalingam[*], Zhengyang Sun[†], Philip O. Scumpia[†], Hilary A. Coller[†], and Aydin Babakhani[*,***]

[*] *Henry Samueli School of Engineering, University of California Los Angeles, Los Angeles, CA, 90095, USA*
[†] *David Geffen School of Medicine at UCLA, Los Angeles, CA, 90095, USA*
[**] *Student Member, IEEE* [***] *Member, IEEE*

Manuscript received May 5, 2020; revised May 24, 2020.

Abstract—In this letter, we present a machine-learning-based solution to classify wounds and normal skin based on a dielectric spectroscopy approach. Using a commercial network analyzer, we have measured the dielectric constant of normal skin and different types of wounds from multiple living mice across a frequency range of 10 MHz to 20 GHz. The acquired data across a wide frequency range is processed by a *Data Dimensionality Reduction* technique to extract the optimum frequency for wound dielectric spectroscopy. The results of our analysis reveal that different types of wounds can be distinguished by acquiring the dielectric constants in a frequency range of 1 GHz to 2 GHz. This finding relaxes the large bandwidth requirements of dielectric spectroscopy sensors. By adopting supervised learning classification tools, we have demonstrated that various tissue types across different samples can be classified with an accuracy of near 100%.

Index Terms—Biosensing, dielectric sensing, dielectric spectroscopy, machine learning, point-of-care diagnostics, wound healing.

I. INTRODUCTION

Each year, an estimated 6.5 million patients in the US experience a wound that fails to heal [1]. Chronic wound management would be revolutionized if doctors could monitor wound healing in real-time remotely and predict accurately which wounds will heal and which will not. To enable a point-of-care solution for wound monitoring, it is essential to develop a low-cost miniaturized sensor device for measuring wound characteristics at different stages of healing [2], [3]. Fig. 1 shows the motivating application for the design of a real-time sensing system for wound monitoring where the measured wound data is wirelessly transferred to a cell phone and uploaded to cloud storage. Ultra-low-power mm-sized data transceivers have been reported recently that conduct data communication with under 5 pJ/b energy efficiency [4]. Hence, the main challenge toward the development of a real-time wound monitoring system is still an integrated solution for characterizing the wound features.

Dielectric spectroscopy is one of the popular methods for characterizing biological tissues due to its non-invasive, label-free, and real-time nature [5]–[9]. Multiple efforts have been done in recent years to realize a miniaturized dielectric spectroscopy sensor [10]–[13]. The common trend in the dielectric spectroscopy sensors has been focused on achieving a large bandwidth. The bandwidth of dielectric sensing systems has been expanded to ensure applicability to various materials. However, the large bandwidth necessitates using microwave components such as waveguides and transmission lines which are large and bulky and may not be feasible to be realized in a CMOS technology. Besides, the power consumption of broadband dielectric sensing devices is in the order of hundreds of milli-Watts which limits their application in low-power and long term applications.

In this paper, we present an experimental study for detecting different types of wound tissue that is jointly based on the dielectric constant measurement and supervised machine learning. The experimental setup for a reliable dielectric constant from an *in-vivo* sample is described in Section II. The recorded data are reported in Section III and the optimum frequency for differentiating wound types is obtained using Principal Component Analysis. Supervised learning tools are used in Section IV to show that the wound and skin dielectric data can be classified with high accuracy in order to facilitate real-time wound monitoring.

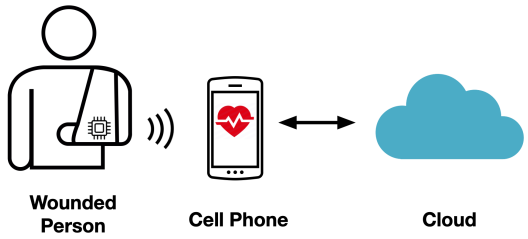

Fig. 1: Operation of a conceptual real-time wound monitoring system.

II. WOUND DIELECTRIC MEASUREMENT SETUP

To evaluate the feasibility of differentiating wound types, a measurement setup is used as shown in Fig. 2. The dielectric constant is measured using a Keysight *N5230C* Vector Network Analyzer (VNA) equipped with a dielectric sensing feature. Dielectric sensing is conducted via a special probe as an extension to the VNA calibration kit. The VNA measures the reflection coefficient between the probe and the sample. Hence, it is essential to calibrate the VNA before the experiment and maintain the calibrated configuration intact during the experiment. To eliminate mechanical vibrations, we used motorized stages to precisely align the probe and the sample. During the experiment, the cable and the probe are fixed to ensure the cable length and formation does not change and the calibration set remains

H. Rahmani, M.M. Archang, and B. Jamali contributed equally to this paper.
Corresponding author: A. Babakhani (e-mail: aydinbabakhani@ucla.edu).
Digital Object Identifier 10.1109/LSENS.2020.0000000

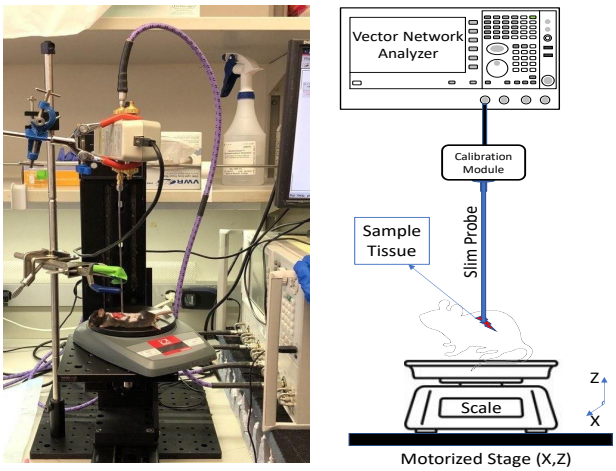

Fig. 2: Measurement setup for obtaining dielectric constant of different types of wounds.

valid. We evaluated the efficacy of the dielectric measurement in differentiating various types of wounds by performing measurements on normal skin and three different wound types: UVB burn, ulcerative dermatitis (UD), and Punch wounds. All animal experiments were conducted in accordance with policies of the NIH Guide for the Care and Use of Laboratory Animals and the approval of the UCLA IACUC (Protocol 2015-031-11). Six black mice were shaved with a 50 clipper and the remaining hair was removed with Nair. For UV wounds, mice were placed inside a UV chamber under a UV resistant cover with a 5mm by 1cm window over their back and exposed to UVB light at 5mJ/s for 10 minutes 2 days prior to performing measurements. During this two-day period, mice scratch the area surrounding the burn, resulting in UD in non-UVB-exposed areas. For punch biopsy a 6mm biopsy punch was used over a fold of skin to create full thickness wounds over flanks, middle back, and neck prior to measurements. Intraperitoneal injection of a ketamine/xylazine mixture at 100/12.5 mg/kg was used for anesthesia during UVB exposure, the introduction of punch wounds, and measurements. Due to the small size of wounds and high degree of curvatures on the mouse body, a slim probe is used for dielectric measurement. The slim probe design features a 2.2 mm aperture than may be used for soft and semi-solid material. However, for an accurate dielectric measurement, flexible material should be gently pressed against the probe to create a well-spread contact that covers the entire probe aperture. Throughout the experiment, we realized that the applied force between the tissue and the probe introduces some variability in the measured dielectric constant values. To eliminate this variable, the sample mouse was placed on a scale during measurement to measure the contact force between probe and animal and adjust it to be equal between measurements.

III. MEASUREMENT RESULTS

The dielectric response of biological tissues to an applied *Alternative Current* (AC) field is captured by a frequency-dependent dielectric constant expressed as :

$$\epsilon(f) = \epsilon^{'}(f) + i \times \epsilon^{''}(f) \quad (1)$$

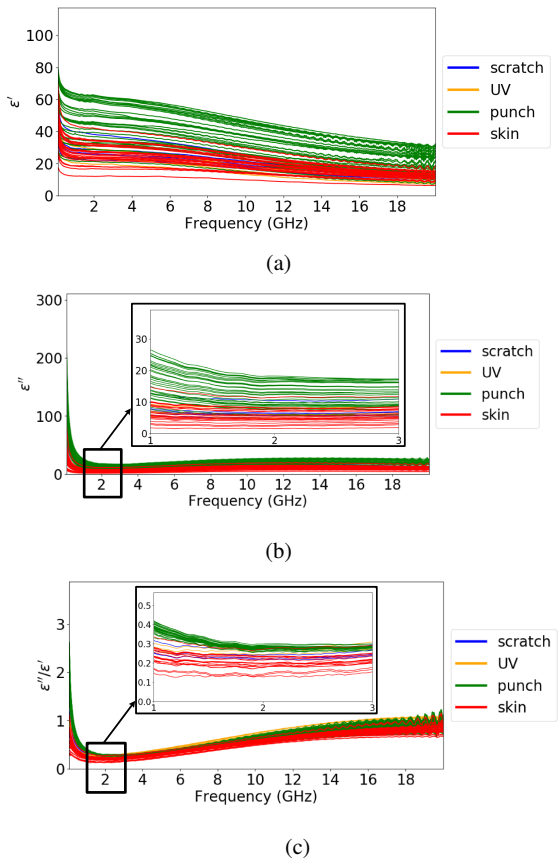

Fig. 3: Measured (a) permittivity, (b) permeability, and (c) loss tangent of the the normal skin and three different wound types.

Table 1: The accuracy of an average-based classification method in correctly classifying the wound and normal skin samples at 2 GHz.

Dielectric Data	Permittivity	Permeability	Loss Tangent
Accuracy	80.3%	83.6%	90.1%

According to (1), the dielectric contestant can be decomposed to a real term and an imaginary term. When a material is excited by an electric field, the real part of the dielectric constant explains the energy storage in the material while the imaginary part describes the energy losses [14]. Different materials can be distinguished by measuring their dielectric constants, also know as dielectric spectroscopy. The measured dielectric constants are plotted in Fig. 3. The ratio of the imaginary part over the real part of the dielectric constant is known as the *loss tangent*. A simple method to classify the measured data into two categories is to define a classification threshold as the mid-point between the average of skin dielectric data and the average of the punch dielectric data at a single frequency. The data on one side of the threshold are classified as normal skin and the data on the other side are classified as wounds. Table 1 reports the accuracy of this method at 2 GHz, defined as the number of correct classifications divided by the number of samples. To achieve a better detection performance and accuracy, other visualization techniques and machine learning classifiers will be used in the remainder of this paper.

The data shown in Fig. 4 represents the original data projected into a lower dimensional space using the first two principal components (PCs) obtained from *Principal Component Analysis* (PCA). The PCA technique allows us to represent a large number of possibly correlated

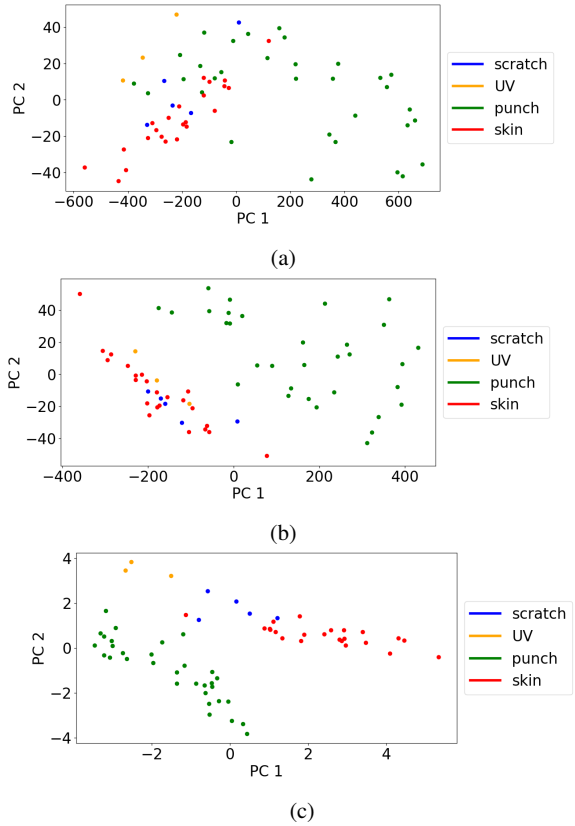

Fig. 4: Two-dimensional plots showing the first two principal components obtained from the Principal Component Analysis (PCA) on the measured (a) permittivity, (b) permeability, and (c) loss tangent.

variables using a smaller set of variables. This smaller collection of variables explains most of the variability in the original data [15]. For visualization purposes, only the first two PCs are used since they represent the top two directions of maximal variance in the data. The top five frequencies with the most contributions to the PCA algorithm are 1.03 GHz, 1.51 GHz, 1.53 GHz, 1.89 GHz, 1.91 GHz. Therefore, the optimum frequency range for designing an integrated dielectric sensor for wound monitoring lies between 1 GHz and 2 GHz. The results shown in Fig. 4 (c) could be used to separate various types of tissues. Hence, a unique probability can be assigned to each region to distinguish the tissue types. This finding could be valuable in a clinical test where a physician can easily detect the wound type based on the measured data.

IV. MACHINE LEARNING AND CLASSIFICATION

To classify the measured data based on the type of skin, the two-dimensional space shown in Fig. 4 (c) needs to be divided into different regions, which set the decision boundaries. Various machine learning tools available in the Scikit-learn library in Python are utilized for this purpose [16]. Fig. 5 visualizes how the two-dimensional space in Fig. 4 (c) is divided into different regions based on the Gaussian distribution of the measured samples. The *Gaussian Mixture Model (GMM)* is an unsupervised learning algorithm that assumes that the distribution of each category converges to a Gaussian distribution as the number of the samples increases. The distribution of the data belonging to each cluster is displayed using different color shades

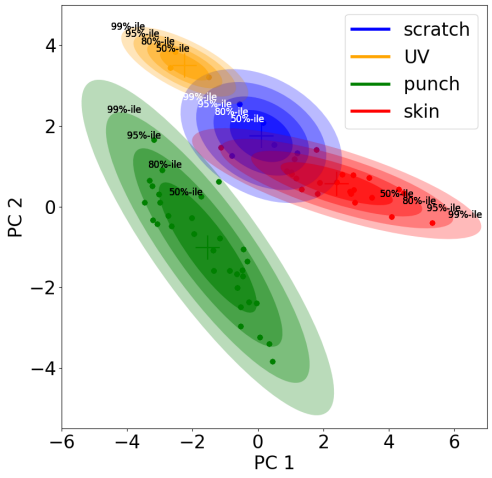

Fig. 5: Clustering of the measured data into four categories using Gaussian Mixture Model.

indicating the percentage of the data within each ellipse. It is observed that the wounds which were created by punch can be clearly separated from the rest of the samples by using the Gaussian process classifier on the electric loss tangent data.

Since the loss tangent data can be successfully clustered by the GMM method, we are motivated to use supervised machine learning methods to divide the PCA data into different regions for classification purposes. Fig. 6 visualizes the decision regions obtained from fitting a Support Vector Classifier (SVC) using different kernel functions and implementations to the PCA-projected data. SVC is a supervised learning algorithm that uses decision boundaries to separate the classes of the data. Traditional SVCs can separate the data using linear decision boundaries. For some classification problems, however, the data may not be linearly separable. SVCs can achieve non-linear decision boundaries by implicitly mapping the data in the original vector space into a higher-dimensional space. When the data is projected in a higher dimensional space, the data may then be linearly separable. The kernel function, which is used for transformation into a higher dimensional space, can be either a higher-degree polynomial or a radial basis function (RBF). Depending on the data, different

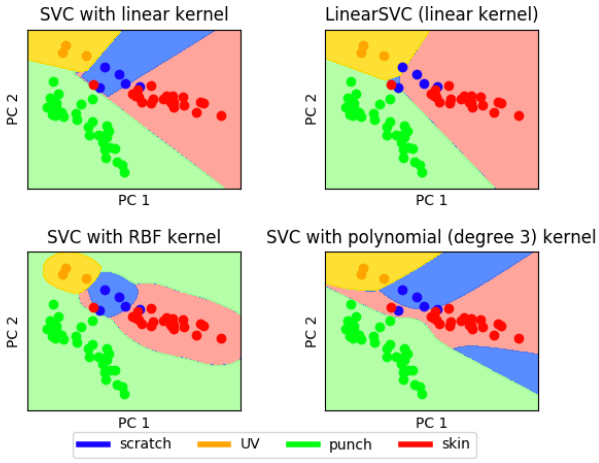

Fig. 6: Support vector classification of the measured data into four categories using different kernel functions.

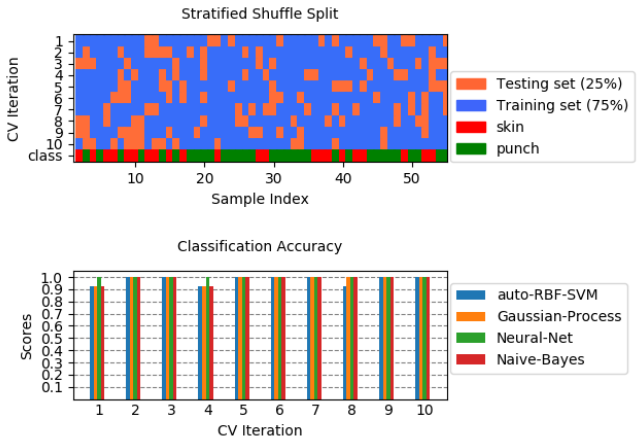

Fig. 7: Classification accuracy in predicting the skin category using different classifiers and various cross-validation iterations.

kernels may provide clearer decision boundaries. These similarity scores computed by the kernel, along with the parameters of the classifier, are used to characterize the decision boundaries [15]. The decision boundaries in the top two plots in Fig. 6 were obtained from fitting LinearSVC and SVC with a linear kernel to the PCA data. Although both of these methods use linear decision boundaries, the former is implemented using the *liblinear* library rather than *libsvm* [16]. This difference in implementation gives the former more flexibility in the choice of loss functions and scales better to a larger number of data points. The bottom two plots were obtained from fitting SVCs that use more complicated kernels. The SVC used in the bottom left plot uses an RBF kernel, while the SVC in the bottom right plot uses a degree-3 polynomial kernel.

In addition to Support Vector Classifier and Supervised Gaussian Process Classifier, Neural Networks and Naive-Bayes Classifier were also trained to assist us in separating skin and wound based on the dielectric measurement results. These four supervised learning tools were trained by the measured dielectric data in order to distinguish skin and wound in classification. Since numerous samples were obtained from wounds created by punch, only this set of data were used as wound samples. In each classification process, 75% of the data were used to train the algorithm and the other 25% were used for testing. The classification accuracy is based on the percentage of the testing data that are assigned to the correct label. The random assignment of different samples to the training and testing data sets were performed using stratified shuttling technique. This shuffling process was done during ten cross-validation iterations to ensure the consistency of the classification accuracy results. The shuffling order in each iteration and their corresponding accuracy results from all four classifiers are reported in Fig. 7. The average classification accuracy for all four classifiers are reported in Table 2, which demonstrates promising results in differentiating wound types based on their dielectric properties. Additional work is needed to establish the efficacy of this method in differentiating different stages of wound healing in additional wound models to establish clinical applicability.

V. CONCLUSION

Dielectric properties of various samples of normal skin and wounds were measured using a vector network analyzer. Principle Component

Table 2: The average cross-validation accuracy in skin/wound classification for different supervised learning tools.

Classifier	SVM	Gaussian Process	Neural Net	Naive Bayes
Accuracy	97.6%	98.4%	100.0%	98.4%

Analysis on the measured loss tangent data shows that different types of wounds can be distinguished from each other and from a normal skin. Supervised learning classification tools were trained by the measured loss tangent data and demonstrated a classification accuracy of near 100% on separating normal skin and the wounds. This study is a first step towards real-time wound monitoring assisted by dielectric sensing and machine learning.

ACKNOWLEDGMENT

This work was funded by the UCLA Broad Stem Cell Research Center innovation award.

REFERENCES

[1] C. K. Sen, G. M. Gordillo, S. Roy, R. Kirsner, L. Lambert, T. K. Hunt, F. Gottrup, G. C. Gurtner, and M. T. Longaker, "Human skin wounds: a major and snowballing threat to public health and the economy," *Wound repair and regen.*, vol. 17, no. 6, pp. 763–771, 2009.

[2] W. Deng, L. Wang, L. Dong, and Q. Huang, "LC Wireless Sensitive Pressure Sensors With Microstructured PDMS Dielectric Layers for Wound Monitoring," *IEEE Sensors J.*, vol. 18, no. 12, pp. 4886–4892, 2018.

[3] C. Occhiuzzi, A. Ajovalasit, M. A. Sabatino, C. Dispenza, and G. Marrocco, "RFID epidermal sensor including hydrogel membranes for wound monitoring and healing," in *2015 IEEE Intl. Conf. RFID (RFID)*, 2015, pp. 182–188.

[4] H. Rahmani and A. Babakhani, "A 1.6mm^3 wirelessly powered reconfigurable FDD radio with on-chip antennas achieving 4.7 pJ/b TX and 1 pJ/b RX energy efficiencies for medical implants," in *Proc. IEEE Custom Integr. Circuits Conf. (CICC)*, Apr. 2020, pp. 1–4.

[5] K. Heileman, J. Daoud, and M. Tabrizian, "Dielectric spectroscopy as a viable biosensing tool for cell and tissue characterization and analysis," *Biosens. and Bioelectron.*, vol. 49, pp. 348–359, 2013.

[6] P. Salvo *et al.*, "Sensors and Biosensors for C-Reactive Protein, Temperature and pH, and Their Applications for Monitoring Wound Healing: A Review," *Sensors*, vol. 17, no. 12, p. 2952, 2017.

[7] C. Gabriel, R. H. Bentall, and E. H. Grant, "Comparison of the dielectric properties of normal and wounded human skin material," *Bioelectromagnetics*, vol. 8, no. 1, pp. 23–27, 1987.

[8] C. Aydinalp, S. Joof, T. Yilmaz, N. P. Özsobaci, F. A. Alkan, and I. Akduman, "In Vitro Dielectric Properties of Rat Skin Tissue for Microwave Skin Cancer Detection," in *Proc. Int. Appl. Comput. Electromagn. Soc. Symp.*, 2019, pp. 1–2.

[9] Y. Gao, M. T. Ghasr, M. Nacy, and R. Zoughi, "Towards Accurate and Wideband In Vivo Measurement of Skin Dielectric Properties," *IEEE Trans. Instrum. Meas.*, vol. 68, no. 2, pp. 512–524, 2019.

[10] M. Bakhshiani, M. A. Suster, and P. Mohseni, "A Broadband Sensor Interface IC for Miniaturized Dielectric Spectroscopy From MHz to GHz," *IEEE J. Solid-State Circuits*, vol. 49, no. 8, pp. 1669–1681, 2014.

[11] M. M. Bajestan, A. A. Helmy, H. Hedayati, and K. Entesari, "A 0.62–10 GHz Complex Dielectric Spectroscopy System in CMOS," *IEEE Trans. Microw. Theory Techn.*, vol. 62, no. 12, pp. 3522–3537, 2014.

[12] J. Chien, M. Anwar, E. Yeh, L. P. Lee, and A. M. Niknejad, "A 1–50 GHz dielectric spectroscopy biosensor with integrated receiver front-end in 65nm CMOS," in *IEEE MTT-S Int. Microw. Symp. Dig.*, 2013, pp. 1–4.

[13] G. Vlachogiannakis, M. Spirito, M. A. P. Pertijs, and L. C. N. de Vreede, "A 40-nm CMOS permittivity sensor for chemical/biological material characterization at RF/microwave frequencies," in *IEEE MTT-S Int. Microw. Symp. Dig.*, 2016, pp. 1–4.

[14] H. Rahmani and A. Babakhani, "A dual-mode RF power harvesting system with an on-chip coil in 180-nm SOI CMOS for millimeter-sized biomedical implants," *IEEE Trans. Microw. Theory Techn.*, vol. 67, no. 1, pp. 414–428, Jan. 2019.

[15] G. James, D. Witten, T. Hastie, and R. Tibshirani, *An introduction to statistical learning*. Springer, 2013, vol. 112.

[16] F. Pedregosa *et al.*, "Scikit-learn: Machine Learning in Python," *J. Mach. Learn. Res.*, vol. 12, pp. 2825–2830, Oct. 2011.